

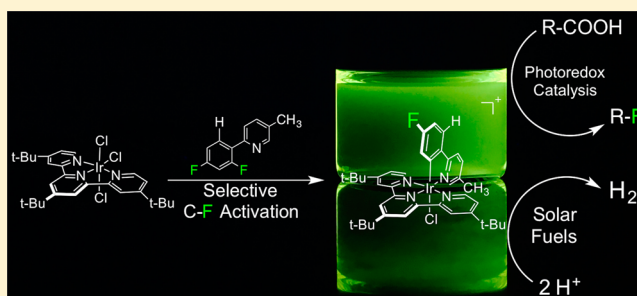
Highly Fluorinated Ir(III)–2,2′:6′,2″-Terpyridine–Phenylpyridine–X Complexes via Selective C–F Activation: Robust Photocatalysts for Solar Fuel Generation and Photoredox Catalysis

Jonathan A. Porras, Isaac N. Mills, Wesley J. Transue, and Stefan Bernhard*

Department of Chemistry, Carnegie Mellon University, Pittsburgh, Pennsylvania 15213, United States

S Supporting Information

ABSTRACT: A series of fluorinated Ir(III)–terpyridine–phenylpyridine–X (X = anionic monodentate ligand) complexes were synthesized by selective C–F activation, whereby perfluorinated phenylpyridines were readily complexed. The combination of fluorinated phenylpyridine ligands with an electron-rich tri-*tert*-butyl terpyridine ligand generates a “push–pull” force on the electrons upon excitation, imparting significant enhancements to the stability, electrochemical, and photophysical properties of the complexes. Application of the complexes as photosensitizers for photocatalytic generation of hydrogen from water and as redox photocatalysts for decarboxylative fluorination of several carboxylic acids showcases the performance of the complexes in highly coordinating solvents, in some cases exceeding that of the leading photosensitizers. Changes in the photophysical properties and the nature of the excited states are observed as the compounds increase in fluorination as well as upon exchange of the ancillary chloride ligand to a cyanide. These changes in the excited states have been corroborated using density functional theory modeling.



INTRODUCTION

Activation of C–F bonds in aromatic and aliphatic compounds has become a prominent route not only for the synthesis of fluorinated organic compounds^{1,2} but also for accessing transition metal complexes that are themselves fluorinated.^{3–13} In order to use C–F activation strategically, understanding the chemoselectivity of the process is necessary.¹⁴ It has been shown that C–H bond activation is typically preferred over C–F bond activation with second- and third-row transition metals, likely because of a higher kinetic barrier despite the fact that C–F activation is energetically favorable.^{15–22} However, there have been a few complexes of Rh and Ir that have shown a preference for C–F activation over C–H activation, likely because oxidative addition/reductive elimination produces a more stable product.^{23–29} It appears that factors such as the oxidation state of the metal center and the kinetic versus thermodynamic preference of the products have significant impacts on controlling the selectivity of such reactions. Ultimately, having control of C–F versus C–H activation is key given that fluorination is a useful strategy for the stabilization and tuning of several second- and third-row transition metal complexes, including Ir(III) complexes.

Ir(III) complexes have seen use in a diverse array of applications ranging from biomedical applications including emissive labels^{30–35} and antitumor drugs³⁶ to photocatalytic applications including photosensitizing water splitting,^{37–39} photosensitizing organic transformations,^{40–48} and dye-sensitized solar cells⁴⁹ to photonic materials applications including

the fabrication of organic light-emitting diodes (OLEDs).^{50–53} Ir(III) complexes have such broad applications and strong performance because of their high phosphorescence quantum efficiency, long excited-state lifetimes, ease of tunability, and ability to be synthesized with a diverse array of ligand functionalities and architectures. All of these properties are consistent with the strong spin–orbit coupling of Ir(III), which gives rise to efficient intersystem crossing from the singlet to the triplet excited state, thereby imparting high phosphorescence efficiencies. Given the ease of tunability of Ir(III) complexes, control of the energies of metal-to-ligand charge transfer (MLCT) and intraligand charge transfer (ILCT) processes can be achieved through modulation of the ligand structure and functionalities. The strategies used to most greatly tune the complexes typically involve decreasing the energy of the highest occupied molecular orbital (HOMO) by introducing electron-withdrawing groups, increasing the energy of the lowest unoccupied molecular orbital (LUMO) by introducing electron-donating groups, and limiting the overall conjugation of the ligands to increase the energy of any π – π^* emissive states.⁵⁴

Several electron-withdrawing moieties have been utilized to tune the energies of the HOMOs in Ir(III) complexes, including sulfonyl,^{55,56} trifluoromethyl,^{57–64} pentafluorosulfur,⁶⁵ trifluoromethoxy,⁶⁶ nitrile,^{67,68} and perfluorocarbonyl

Received: March 29, 2016

Published: July 7, 2016

groups.⁶⁹ While such functional groups have resulted in excellent modulation of the HOMO levels in Ir(III) complexes, their implementation into ligand structures and the ability to utilize more than one in a single ligand complicates their use. In contrast, fluorine is significantly simpler to implement into ligand structures and therefore can be used to more easily tune the energy levels by control of the number of fluorine atoms. Therefore, synthesizing complexes with varying degrees of fluorination is paramount to understanding the effects on the energy levels, properties, and catalytic activity within a series of complexes. Ideally, perfluorinated complexes should display the most dramatic difference in terms of the orbital energy levels and should be investigated. While several highly fluorinated Ir(III) complexes have been published,^{70–72} their syntheses have relied on the reaction with an asymmetrical polyfluorinated phenylpyridine ligand or depended on the use of directing groups that would promote Ir(III) cyclometallation,⁷³ further complicating their synthesis. Therefore, a simplified protocol to include highly fluorinated symmetrical ligands into Ir(III) complexes would be advantageous.

The ligand architecture $[\text{Ir}(\text{tpy})(\text{ppy})\text{X}]^+$ (tpy = terpyridine, ppy = phenylpyridine, X = monodentate ligand) has only recently gained attention because of its overall enhanced stability, improved photophysical properties, and diverse catalytic applications.^{74–78} It is advantageous that the HOMO and LUMO are well-partitioned within the structures. Specifically, the HOMO is primarily located on the cyclometallating ligand and the ancillary ligand, and the LUMO is predominantly positioned on the tridentate ligand. Utilizing an electron-rich tridentate ligand with a strongly electron-withdrawing cyclometallating ligand efficiently creates a “push–pull” force on the electrons upon excitation. In this work, a series of such “push–pull”-type complexes are shown to have photophysical and electrochemical properties that are directly impacted by differing degrees of fluorination as well as the strength of the ancillary ligand. To achieve various degrees of fluorination, the complexes were synthesized utilizing C–F activation, which has not been used as a deliberate synthetic tool for Ir(III) complexes. In implementing C–F activation, this work shows high selectivity in the specific stereoisomer that is formed in the cyclometallating reaction. As a result, the synthesis of complexes with perfluorophenyl ligands has been drastically simplified. Details of the electronic structure of the complexes are collected through computational modeling, photophysical spectroscopy, and electrochemical experiments. Finally, the complexes are evaluated for catalytic applications, including photocatalytic hydrogen evolution and redox photocatalysis of decarboxylative fluorination of carboxylic acids.

■ EXPERIMENTAL SECTION

General. The compounds 4,4',4''-tri-*tert*-butyl-2,2':6',2''-terpyridine (ttbutpy) and $\text{IrCl}_3 \cdot 4\text{H}_2\text{O}$ and all of the solvents were used as received from commercial sources. The ligands 5-methyl-2-phenylpyridine (mppy), 2-(4-fluorophenyl)-5-methylpyridine (4-Fmppy), 2-(2-fluorophenyl)-5-methylpyridine (2-Fmppy), 2-(2,4-difluorophenyl)-5-methylpyridine (2,4-dFmppy), 2-(2,6-difluorophenyl)-5-methylpyridine (2,6-dFmppy), and 5-methyl-2-(2,4,6-trifluorophenyl)pyridine (2,4,6-tFmppy) were prepared from the corresponding acylpyridinium salts as described by Lowry et al.³⁸ The ligands 5-methyl-2-(perfluorophenyl)pyridine (PFmppy) and 5-methoxy-2-(perfluorophenyl)pyridine (PFMeOppy) were prepared using the procedure described by Do and Daugulis.⁷⁹ ^1H , ^{13}C , and ^{19}F NMR spectra were obtained using Bruker Avance 300 and 500 MHz spectrometers. ^1H and ^{13}C NMR spectra were referenced to residual

solvent signals. ^{19}F NMR spectra were referenced to CFCl_3 using the PF_6^- anion (−71.11 ppm, doublet) as an internal standard. Electrospray ionization mass spectrometry (ESI-MS) was performed with 50 μM methanol solutions using a Thermo-Fisher LCQ instrument. Elemental analyses were conducted by Robertson Microлит Laboratories (Ledgewood, NJ).

Electrochemistry. Cyclic voltammetry experiments were performed using a CH-Instruments Electrochemical Analyzer 600C potentiostat with a three-electrode system consisting of a platinum coil counter electrode, a silver wire pseudoreference electrode, and a 1 mm^2 platinum disk working electrode. Scans were performed with positive scan polarity at 0.10 V/s under an atmosphere of argon using argon-purged acetonitrile solutions that contained 0.10 M tetra-*n*-butylammonium hexafluorophosphate as the supporting electrolyte and 0.5 mM analyte. An internal standard of ferrocene was added to each solution, and the potentials were referenced to SCE via the oxidation of ferrocene at 0.40 V.⁸⁰

Computational Methodology. Density functional theory (DFT) calculations were performed using the Gaussian 09 suite.⁸¹ The triplet and singlet ground and excited states were evaluated for the complexes using the B3LYP functional and the LANL2DZ basis set. No symmetry conditions were specified. For time-dependent DFT (TD-DFT) calculations, the optimized singlet-ground-state geometry was used for the 150 lowest excitations and solvent (acetonitrile) was specified. Orbitals were visualized using the open-source molecular builder and visualization tool Avogadro, version 1.1.1.⁸² TD-DFT calculations of UV–vis absorption spectra were visualized using Gausssum,⁸³ where transitions were expanded into Gaussian curves with the full width at half-maximum set to 4000 cm^{-1} .

Photophysical Characterization. Room-temperature photophysical measurements were conducted using argon-purged 10 μM acetonitrile solutions in screw-top quartz cuvettes. UV–vis absorption spectra were collected with a Shimadzu UV-1800 spectrophotometer. Photoluminescence characterization experiments were performed using a Fluorolog-3 spectrophotometer equipped with dual monochromators and a photomultiplier tube at a right-angle geometry. All of the compounds were excited at 380 nm. Excited-state lifetimes were determined by pulsing samples at 266 nm using the fourth harmonic of a Continuum Minilite II Nd:YAG laser. Emission decays were monitored with an oscilloscope (Tektronix TDS 3032B) and converted into a linear regression using a LabVIEW PC interface. Emission quantum yields were determined by comparison against a 10 μM $[\text{Ru}(\text{bpy})_3](\text{PF}_6)_2$ reference in acetonitrile, with an established quantum yield ($\phi_{\text{ref}} = 0.062$).⁸⁴ Quantum yields were calculated using the equation $\phi_s = \phi_{\text{ref}}(I_s/I_{\text{ref}})(A_{\text{ref}}/A_s)(\eta_s/\eta_{\text{ref}})$, where ϕ_s is the quantum yield of the sample, ϕ_{ref} is the quantum yield of the reference, I_s and I_{ref} are the maximum emission intensities for the sample and the reference, A_s and A_{ref} are the absorbances of the sample and reference at the excitation wavelength, and η_{ref} and η_s are the refractive indices of the solvents. Radiative decay constants (k_r) were calculated using the equation $k_r = \phi_s/\tau_s$, where τ_s is the excited-state lifetime of the sample, and subsequently, nonradiative decay constants (k_{nr}) were calculated using the relationship $k_{\text{nr}} = (1/\tau_s) - k_r$. Emission intensities were corrected for the detector's response over the spectral range.

Photocatalytic Hydrogen Generation. Photocatalytic generation of H_2 was carried out using the fixed protocol described by Cline et al.⁸⁵ Screw-top EPA vials (40 mL) contained 10 mL of solvent (8 mL of acetonitrile, 1 mL of triethylamine, 1 mL of water), 0.075 mM photosensitizer, and 300 nmol of K_2PtCl_4 . Control vials were prepared without the photosensitizer, the catalyst, or trimethylamine or with all of the components present but without illumination. The vials were placed in a 16-well temperature-controlled photoreactor mounted on an orbital shaker. Each vial was equipped with a pressure transducer as well as a bottom LED for illumination (Luxeon V Dental blue LEDs (LXHL-LRD5) with Fraen collimating optics (FHS-HNBI-LL01-H)). The vials were sealed and subsequently degassed with seven cycles of vacuum and argon, after which the vials were equilibrated to atmospheric pressure at 22 °C. The orbital shaker was started (100 rpm), and the samples were illuminated. Generation of H_2 was monitored over time by conversion of the pressure transducer readings

into pressure traces via a LabVIEW PC interface. Illumination ceased when no further increase in the traces was observed. Following illumination, quantification of the H_2 produced was accomplished by injecting 1 mL of the vial headspace into a GOW-MAC gas chromatograph (thermal conductivity detector, Ar carrier gas) that was precalibrated using 10% H_2 /Ar gas mixtures.

Photoredox Catalysis. The photoredox catalysis studies were performed using a modified version of the reaction conditions reported by Ventre et al.⁸⁶ Screw-top EPA vials (20 mL) containing 5.1 mL of solvent (3:1 acetonitrile/water), 510 μ mol of the corresponding carboxylic acid, 1.02 mmol of Na_2HPO_4 , 1.53 mmol of Selectfluor[®] reagent, and 0.255 μ mol (0.05 mol %) of photosensitizer were equipped with pressure transducers in a 16-well temperature-controlled photoreactor on top of an orbital shaker. Samples were degassed with seven cycles of vacuum and argon, after which the vials were equilibrated to atmospheric pressure. The orbital shaker was started (100 rpm), and the samples were illuminated from the bottom (Luxeon V Dental blue LEDs with Fraun collimating optics) at 22 °C. Generation of CO_2 was monitored over time by conversion of the pressure transducer readings into pressure traces via a LabVIEW PC interface. Illumination ceased after 3 h. The crude reaction mixtures were directly analyzed by ^{19}F NMR spectroscopy using hexafluorobenzene as an internal standard.

Synthesis of $[Ir(ttbutpy)Cl_3]$ (1a**).** In a 40 mL EPA vial, $IrCl_3 \cdot 4H_2O$ (321 mg, 0.800 mmol), 4,4',4''-tri-*tert*-butyl-2,2':6',2''-terpyridine (326 mg, 0.880 mmol, 1.10 equiv), and a stir bar were purged with argon for 15 min before the injection of 13 mL of ethylene glycol. The vessel was purged with argon for an additional 10 min and then stirred for 22 min at 160 °C in a preheated aluminum heating block in the dark. Once cooled, the reaction mixture was diluted with 25 mL of water, and the red precipitate was collected on a Büchner funnel and washed with water and diethyl ether. Yield: 86%. 1H NMR (500 MHz, $DMSO-d_6$): δ 9.06 (m, 2H), 8.86 (m, 2H), 8.79 (m, 2H), 7.96 (m, 2H), 1.79 (m, 9H), 1.47 (m, 18H). Concentrations necessary for ^{13}C NMR spectroscopy could not be obtained because of the poor solubility of **1a** in $DMSO-d_6$.

Synthesis of $[Ir(ttbutpy)(mppy)Cl](PF_6)$ Complexes. In a typical reaction, a 40 mL EPA vial was charged with $[Ir(ttbutpy)Cl_3]$ (50 mg, 0.071 mmol), cyclometalating ligand (0.213 mmol, 3.00 equiv), and a stir bar. The vessel was purged with argon for 15 min, after which 13 mL of ethylene glycol was injected and the vessel was purged for an additional 10 min. The reaction mixture was stirred at 183 °C in a preheated aluminum heating block in the dark for 18 h. Once cooled, the reaction mixture was diluted with 20 mL of water, sonicated, and filtered through a pad of Celite, and the filtrate was poured into a 125 mL separatory funnel. The water/ethylene glycol mixture was extracted with diethyl ether (5 \times 25 mL). The aqueous phase was gently heated in a 40 °C water bath to remove residual diethyl ether before the addition of ~300 mg of KPF_6 . The mixture was stirred for 1 h at room temperature, after which the complex was isolated on a Büchner funnel and washed with water and diethyl ether. The complex was then purified by evaporation of methanol from a methanol/water mixture.

$[Ir(ttbutpy)(mppy)Cl](PF_6)$ (**2a**). Yield: 44%. 1H NMR (500 MHz, acetone- d_6): δ 9.96 (s, 1H), 8.97 (s, 2H), 8.79 (s, 2H), 8.35 (d, J = 8.36 Hz, 1H), 8.14 (d, J = 8.31 Hz, 1H), 7.88 (d, J = 7.77 Hz, 1H), 7.72 (d, J = 6.02 Hz, 2H), 7.55 (dd, J = 1.88, 6.02 Hz, 2H), 6.95 (t, J = 7.48 Hz, 1H), 6.74 (t, J = 7.42 Hz, 1H), 6.11 (d, J = 7.60 Hz, 1H), 2.63 (s, 3H), 1.65 (s, 9H), 1.40 (s, 18H). ^{19}F NMR (470.54 MHz, acetone- d_6): δ -71.11 (d, J = 707.62 Hz, $[PF_6^-]$). ^{13}C NMR (125.77 MHz, acetone- d_6): δ 166.0, 165.6, 164.9, 159.4, 156.6, 152.3, 151.7, 145.3, 142.8, 141.6, 135.3, 131.6, 130.9, 126.4, 125.7, 124.9, 124.1, 122.6, 120.9, 37.6, 36.6, 31.1, 30.5, 18.7. MS (m/z ESI, CH_3OH): calcd 797.3 $[M - PF_6^-]^+$, found 797.4 $[M - PF_6^-]^+$. Anal. Calcd for $[C_{39}H_{45}ClF_6IrN_4P] \cdot 1/2 H_2O$: C, 49.47; H, 4.84; N, 5.92. Found: C, 49.45; H, 4.87; N, 5.72.

$[Ir(ttbutpy)(4-Fmppy)Cl](PF_6)$ (**2b**). Yield: 33%. 1H NMR (500 MHz, acetone- d_6): δ 9.92 (s, 1H), 8.98 (s, 2H), 8.81 (s, 2H), 8.32 (d, J = 8.36 Hz, 1H), 8.15 (d, J = 8.32 Hz, 1H), 7.97 (dd, J = 5.59, 8.56 Hz, 1H), 7.72 (d, J = 6.00 Hz, 2H), 7.56 (dd, J = 1.96, 6.01 Hz, 2H), 6.73

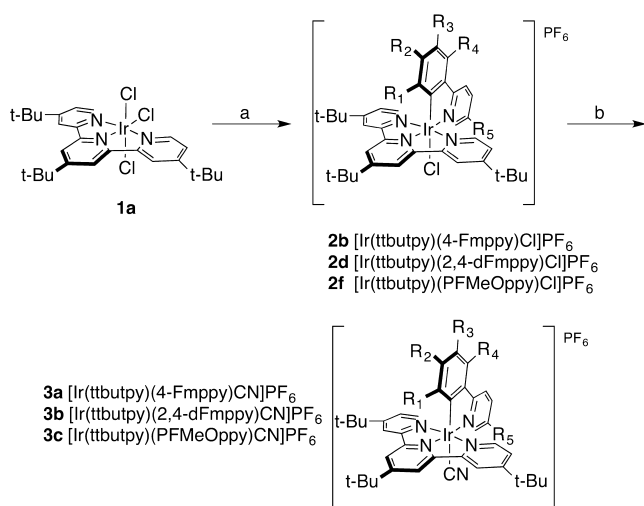
(td, J = 2.42, 8.86 Hz, 1H), 5.79 (dd, J = 2.38, 8.99 Hz, 1H), 2.62 (s, 3H), 1.66 (s, 9H), 1.40 (s, 18H). ^{19}F NMR (470.54 MHz, acetone- d_6): δ -71.11 (d, J = 707.35 Hz, $[PF_6^-]$), -109.17 (s, 1F). ^{13}C NMR (125.77 MHz, acetone- d_6): δ 166.2, 165.7, 163.9, 163.4 (d, J = 252.9 Hz), 159.2, 156.4, 152.2, 151.5, 146.02 (d, J = 5.6 Hz), 141.7, 141.8 (d, J = 2.2 Hz), 135.1, 127.6 (d, J = 9.1 Hz), 126.4, 124.2, 122.8, 120.9, 117.8 (d, J = 18.3 Hz), 111.7 (d, J = 22.7 Hz), 37.6, 36.5, 31.0, 30.4, 18.6. MS (m/z ESI, CH_3OH): calcd 815.3 $[M - PF_6^-]^+$, found 815.5 $[M - PF_6^-]^+$. Anal. Calcd for $[C_{39}H_{44}ClF_7IrN_4P]$: C, 48.77; H, 4.62; N, 5.83. Found: C, 49.53; H, 4.61; N, 5.80.

$[Ir(ttbutpy)(2-Fmppy)Cl](PF_6)$ (**2c**). Yield: 61%. 1H NMR (500 MHz, acetone- d_6): δ 10.05 (s, 1H), 8.97 (s, 2H), 8.80 (m, 2H), 8.47 (d, J = 8.51 Hz, 1H), 8.18 (d, J = 8.37 Hz, 1H), 7.74 (d, J = 6.01 Hz, 2H), 7.55 (dd, J = 1.88, 6.00 Hz, 2H), 6.78 (m, 1H), 6.72 (dd, J = 8.18, 12.42 Hz, 1H), 5.95 (m, 1H), 2.64 (s, 3H), 1.64 (s, 9H), 1.39 (s, 18H). ^{19}F NMR (470.54 MHz, acetone- d_6): δ -71.11 (d, J = 707.35 Hz, $[PF_6^-]$), -112.54 (s, 1F). ^{13}C NMR (125.77 MHz, acetone- d_6): δ 166.2, 165.7, 162.0, 161.0 (d, J = 264.3 Hz), 159.2, 156.4, 152.3, 152.2, 145.1, 141.8, 135.6, 132.6 (d, J = 5.5 Hz), 132.1 (d, J = 8.9 Hz), 127.5 (d, J = 2.8 Hz), 126.4, 124.8 (d, J = 19.7 Hz), 124.2, 122.6, 112.1 (d, J = 22.7 Hz), 37.6, 36.5, 31.0, 30.4, 18.6. MS (m/z ESI, CH_3OH): calcd 815.3 $[M - PF_6^-]^+$, found 815.4 $[M - PF_6^-]^+$. Anal. Calcd for $[C_{39}H_{44}ClF_7IrN_4P] \cdot H_2O$: C, 47.87; H, 4.74; N, 5.73. Found: C, 47.27; H, 4.34; N, 5.52.

$[Ir(ttbutpy)(2,4-dFmppy)Cl](PF_6)$ (**2d**). Yield: 39%. 1H NMR (500 MHz, acetone- d_6): δ 10.02 (d, J = 1.99 Hz, 1H), 8.99 (s, 2H), 8.82 (s, 2H), 8.43 (d, J = 9.17 Hz, 1H), 8.20 (d, J = 10.32 Hz, 1H), 7.74 (d, J = 6.01 Hz, 2H), 7.57 (dd, J = 2.12, 6.05 Hz, 2H), 6.65 (ddd, J = 2.32, 9.31, 11.81 Hz, 1H), 5.70 (dd, J = 2.30, 8.12 Hz, 1H), 2.64 (s, 3H), 1.65 (s, 9H), 1.40 (s, 18H). ^{19}F NMR (470.54 MHz, acetone- d_6): δ -71.11 (d, J = 707.34 Hz, $[PF_6^-]$), -106.61 (d, J = 9.98 Hz, 1F), -108.82 (d, J = 10.00 Hz, 1F). ^{13}C NMR (125.77 MHz, acetone- d_6): δ 166.5, 165.9, 164.3 (d, J = 12.5 Hz), 161.8 (dd, J = 110.3, 9.7 Hz), 160.2 (d, J = 12.8 Hz), 159.2, 156.3, 152.3, 152.1, 147.5 (d, J = 6.6 Hz), 142.0, 135.6, 129.3 (dd, J = 5.3, 3.0 Hz), 126.5, 124.4, 124.2, 122.9, 114.3 (dd, J = 18.1, 3.0 Hz), 100.7 (t, J = 27.0 Hz), 37.6, 36.6, 31.0, 30.5, 18.6. MS (m/z ESI, CH_3OH): calcd 833.3 $[M - PF_6^-]^+$, found 833.4 $[M - PF_6^-]^+$. Anal. Calcd for $[C_{39}H_{43}ClF_8IrN_4P] \cdot 1/2 H_2O$: C, 47.44; H, 4.49; N, 5.67. Found: C, 47.35; H, 4.13; N, 5.60.

$[Ir(ttbutpy)(PFmppy)Cl](PF_6)$ (**2e**). Yield: 36%. 1H NMR (500 MHz, acetone- d_6): δ 10.05 (s, 1H), 8.95 (s, 2H), 8.83 (s, 2H), 8.49 (d, J = 8.50 Hz, 1H), 8.27 (d, J = 8.47 Hz, 1H), 7.74 (d, J = 6.02 Hz, 2H), 7.59 (dd, J = 2.06, 6.02 Hz, 2H), 2.65 (s, 3H), 1.64 (s, 9H), 1.42 (s, 18H). ^{19}F NMR (470.54 MHz, acetone- d_6): δ -71.11 (d, J = 707.39 Hz, $[PF_6^-]$), -134.11 (dd, J = 14.95, 25.13 Hz, 1F), -139.46 (ddd, J = 5.11, 15.09, 24.51 Hz, 1F), -153.34 (ddd, J = 5.05, 18.90, 24.51 Hz, 1F), -162.29 (t, J = 19.16 Hz, 1F). ^{13}C NMR (125.77 MHz, acetone- d_6): δ 166.5, 166.2, 161.1 (m), 159.7, 156.8, 152.3 (d, J = 17.3 Hz), 152.7, 152.4, 142.2, 136.9, 126.6, 126.5 (d, J = 3.0 Hz), 125.4 (d, J = 19.8 Hz), 124.2, 124.1, 124.0 (d, J = 8.0 Hz), 122.2, 122.1 (t, J = 5.48 Hz), 118.3 (d, J = 79.5 Hz), 37.5, 36.6, 31.0, 30.5, 18.7. MS (m/z ESI, CH_3OH): calcd 869.2 $[M - PF_6^-]^+$, found 869.5 $[M - PF_6^-]^+$. Anal. Calcd for $[C_{39}H_{41}ClF_{10}IrN_4P] \cdot 1/2 H_2O$: C, 45.77; H, 4.14; N, 5.47. Found: C, 45.73; H, 3.93; N, 5.37.

$[Ir(ttbutpy)(PFMeOppy)Cl](PF_6)$ (**2f**). Yield: 50%. 1H NMR (500 MHz, acetone- d_6): δ 9.99 (d, J = 2.83 Hz, 1H), 8.95 (s, 2H), 8.84 (d, J = 1.85 Hz, 2H), 8.52 (dd, J = 1.21, 9.28 Hz, 1H), 8.05 (dd, J = 2.77, 9.12 Hz, 1H), 7.80 (d, J = 5.97 Hz, 2H), 7.59 (dd, J = 2.13, 6.05 Hz, 2H), 4.14 (s, 3H), 1.64 (s, 9H), 1.42 (s, 18H). ^{19}F NMR (470.54 MHz, acetone- d_6): δ -71.11 (d, J = 707.37 Hz, $[PF_6^-]$), -134.37 (dd, J = 14.84, 25.16 Hz, 1F), -141.04 (ddd, J = 4.34, 14.90, 19.33 Hz, 1F), -154.43 (ddd, J = 4.30, 18.86, 23.85 Hz, 1F), -162.37 (t, J = 19.14 Hz, 1F). ^{13}C NMR (125.77 MHz, acetone- d_6): δ 166.6, 166.3, 159.7, 157.5 (d, J = 0.4 Hz), 156.8, 156.2 (m), 152.5, 152.4 (d, J = 6.4 Hz), 146.7 (m), 144.8 (m), 140.7, 130.0 (m), 124.2 (d, J = 29.4 Hz), 126.6 (d, J = 19.8 Hz), 126.5, 126.0, 122.3 (d, J = 5.0 Hz), 122.2, 117.4 (d, J = 34 Hz), 57.2, 37.6, 36.5, 31.0, 30.5. MS (m/z ESI, CH_3OH): calcd 885.3 $[M - PF_6^-]^+$, found 885.4 $[M - PF_6^-]^+$. Anal. Calcd for

Scheme 2. Chloride–Cyanide Exchange of Ir(III) Complexes^a

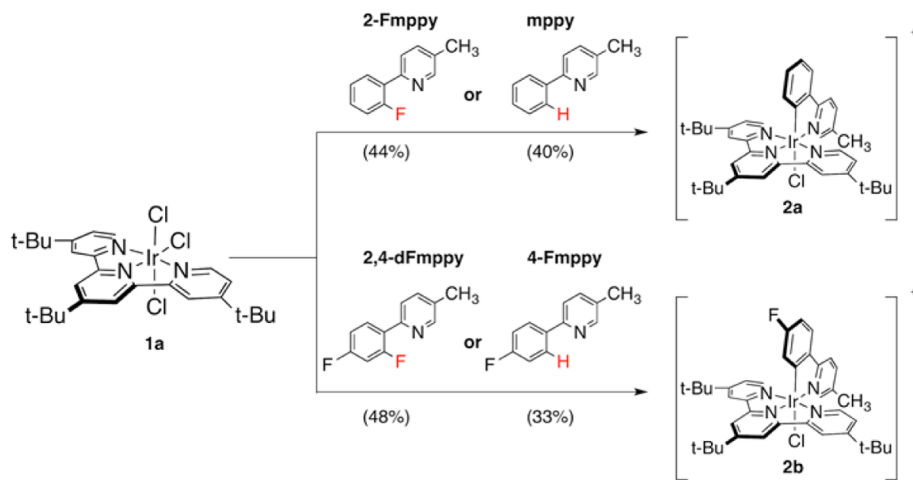
^aReaction conditions: (a) mppy ligand, ethylene glycol, argon atmosphere, 182 °C, overnight; (b) KCN(aq), ethylene glycol, argon atmosphere, 90 °C, 2 h.

The mppy ligand derivatives were synthesized via Kröhnke condensation of the corresponding phenylacetylpyridinium salt with methacrolein³⁸ or via CuI-catalyzed cross-coupling of pentafluorobenzene with the corresponding 2-bromopyridine precursor.⁷⁹

The addition of electronegative fluorine atoms to the mppy ligand was needed in order to achieve the desired “push–pull” design by altering the HOMO energy level of the complexes. It has been thought that cyclometallations of Ir(III) with mppy-type ligands have shown a preference for C–H over C–F activation with ortho-fluorinated mppy ligands. However, in the reaction of 2,4-dFmppy with **1a**, the monofluorinated complex **2b** was the primary product, with small quantities of the difluorinated complex **2d** detected by analysis of the crude reaction mixture with ¹⁹F NMR spectroscopy and ESI-MS (see the Supporting Information). A similar behavior was observed

in the reaction of **1a** with 2-Fmppy, whereby the C–F activation product **2a** was the reaction product, with small quantities of the monofluorinated **2c** detected by ¹⁹F NMR spectroscopy and ESI-MS (see the Supporting Information). Purification of these products by crystallization after precipitation of the PF₆ salt did produce only the pure C–F activation products. To synthesize **2d**, 2,4,6-tFmppy was instead used as the cyclometallating ligand, whereas to synthesize **2c**, 2,6-dFmppy was used. C–F activation was also observed by the formation of the perfluorinated complexes when pentafluorophenyl ligands were used. Given the preference of C–F activation over C–H activation, it was then possible to synthesize complexes **2a** and **2b** using C–F or C–H activation, as shown in Scheme 3. It should be noted that the yields of the reactions using C–F activation were comparable in the synthesis of **2a** (44% using 2-Fmppy and 40% using mppy) but were significantly higher in the synthesis of **2b** (48% using 2,4-dFmppy vs 33% for 4-Fmppy). In all cases, the ancillary ligand of the complexes synthesized via C–F activation remained a chloride and was not exchanged to fluoride, as confirmed by ¹⁹F NMR spectroscopy and mass spectrometry. Over the course of the reaction, the Ir(III) precursor is transiently reduced to Ir(I), oxidizing the ethylene glycol solvent and liberating protons. These liberated protons react with the fluoride produced by the C–F insertion, generating hydrofluoric acid, which was then shown to react with borosilicate glass reaction vials by the appearance of BF₄[−] and BF₃OH[−] detected via ¹⁹F NMR spectroscopy of the crude reaction mixture (see the Supporting Information).⁸⁷ Formation of SiF₆^{2−} was anticipated,⁸⁸ but it could not be detected by ¹⁹F NMR spectroscopy.

The preference for C–F activation of the complexes over C–H activation is likely due to the formation of Ir(I) species typically generated during cyclometallation reactions performed in oxidizable solvents and the elevated reaction temperatures favoring C–F over C–H activation. In the presence of oxidizable ethylene glycol, **1a** is likely reduced to a transient Ir(I) species, which upon oxidative addition to a fluorinated mppy ligand is then reoxidized to the final Ir(III) species. At the elevated reaction temperatures, thermodynamic control of

Scheme 3. Syntheses of **2a** and **2b** Using C–F and C–H Activation under Identical Reaction Conditions^a

^aIsolated yields are shown in parentheses. Note: The C–F activation products were the major products of the reactions, with trace amounts of the C–H products being detected by ¹⁹F NMR and ESI-MS analyses of the crude reaction mixtures (see the Supporting Information). Crystallization furnished only the pure C–F activation products.

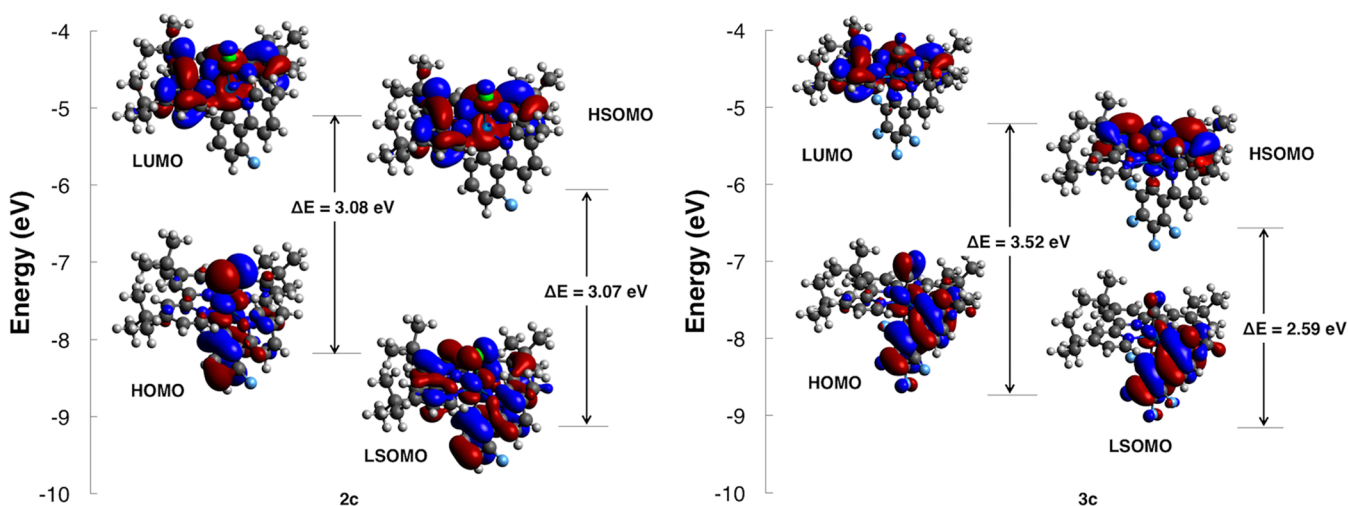


Figure 1. Frontier orbitals of (left) **2c** and (right) **3c** from Gaussian 09 DFT calculations. A notable reduction in the metal character of the LUMO, highest singly occupied MO (HSOMO), and lowest singly occupied MO (LSOMO) is observed in going from the monofluorinated chloro complex **2c** to the perfluorinated cyano complex **3c**. The HSOMO \rightarrow LSOMO transition in **2c** has mixed MLCT/ILCT character, whereas in **3c** the loss of metal character results in the transition having primarily ILCT character.

the products would produce more of the C–F activation product over the C–H product. To better understand the reaction, attempts to identify the oxidized products were made by reaction with 2,4-dinitrophenylhydrazine followed by ^1H NMR characterization of the corresponding hydrazones that precipitated from the solution (see the [Supporting Information](#)). While the product corresponded to the hydrazone formed from the reaction with glyoxal, the origin of the glyoxal from the oxidation by the Ir could not be distinguished from the oxidation of the solvent by residual oxygen in the reaction or from that which originated from solvent oxidation over time at elevated temperatures, making additional detailed characterizations and quantifications difficult. Control reactions using solvents that are inert to oxidation, including 2,3-dimethyl-2,3-butanediol, 2,5-dimethyl-2,5-hexanediol, and *tert*-butyl alcohol were inconclusive since the lower solubility of the starting materials could have prevented any C–F activation from occurring. Attempts to run the reactions at lower temperatures were made, but no reaction occurred, indicating an elevated energy barrier for the reaction.

It should be noted that Huang et al.³¹ recently performed a similar reaction of $[\text{Ir}(p\text{-tolyl-tpy})\text{Cl}_3]$ (*p*-tolyl-tpy = 4'-(4-methylphenyl)-2,2':6',2''-terpyridine) with 2,4-dFppy and mischaracterized the product as the difluorinated $[\text{Ir}(p\text{-tolyl-tpy})(2,4\text{-dFppy})\text{Cl}]^+$. Closer inspection of mass spectrometry experiments revealed a trace amount of the difluorinated (C–H activation product) in the presence of the primarily monofluorinated (C–F activation product). Similar ratios of the C–F and C–H products were observed in mass spectrometry experiments conducted in this work (see the [Supporting Information](#)). While the ^1H NMR and elemental analyses of the product could correspond to the C–H activation product, the lack of ^{19}F NMR and ^{13}C NMR analyses, whereby mono- versus difluorination would be most obvious, makes identification of the reaction product difficult.

Computational Modeling. The electronic structures and geometries of the complexes were modeled using DFT calculations, specifically with the B3LYP functional and the LANL2DZ basis set for the singlet and triplet states. The frontier orbitals of the singlet and triplet states of the

monofluorinated chloro complex **2c** and the perfluorinated cyano complex **3c** are depicted in [Figure 1](#). The LUMO of each complex is located primarily on the terpyridine ligand with contributions from the d orbitals of the metal center, as a result of the strongly electron-donating *tert*-butyl groups on the terpyridine. The HOMO of each complex displays contributions from the phenyl ring of the mppy ligand, the iridium d orbitals, and the ancillary ligand.

For the chloro complexes, as the mppy ligand increases in fluorination, the electronic structure of the LUMO remains unchanged. However, in the cyano complexes, the LUMO shows a decrease in metal character as the complex increases in fluorination (see the [Supporting Information](#)). The electronic structure of the HOMO of the chloro complexes shows an increase in the electron density of the phenyl ring in the mppy ligand with increasing fluorination. A similar trend is observed in the cyano complexes. The addition of a methoxy group to the pyridine ring in chloro complex **2f** and cyano complex **3c** results in a significant increase in the contribution of the pyridine ring to the HOMO.

As the chloro complexes become more fluorinated, the HOMO energy levels of the complexes are lowered compared with the unsubstituted complex **2a**. Fluorination also results in a broadening of the HOMO–LUMO gap within a 0.36 eV range for the chloro complexes. Both of these trends are also seen in the corresponding cyano complexes. Exchange of the chloride to a stronger-field cyanide ligand results in a decrease in the HOMO levels by 0.26 eV as well as broadening of the HOMO–LUMO gaps.

UV–Vis Absorption Spectroscopy. The absorption spectra of complexes **2b**, **2f**, and **3c** collected in acetonitrile are shown in [Figure 2](#). Complex **2b**'s spectrum is representative of the spectra of **2a–d**, whereas **2f** is representative of the perfluorinated chloro complexes. The spectrum of **3c** is representative of the cyano complexes **3a–c**. All of the photophysical properties are presented in [Table 1](#). The spectra of chromophores with an $[\text{Ir}(\text{tpy})(\text{ppy})\text{X}]^+$ ligand structure and the origins of the observed transitions are similar to published spectra,⁷⁴ as indicated by TD-DFT calculations (Figures S35–S37 in the [Supporting Information](#)). A weak feature near 475

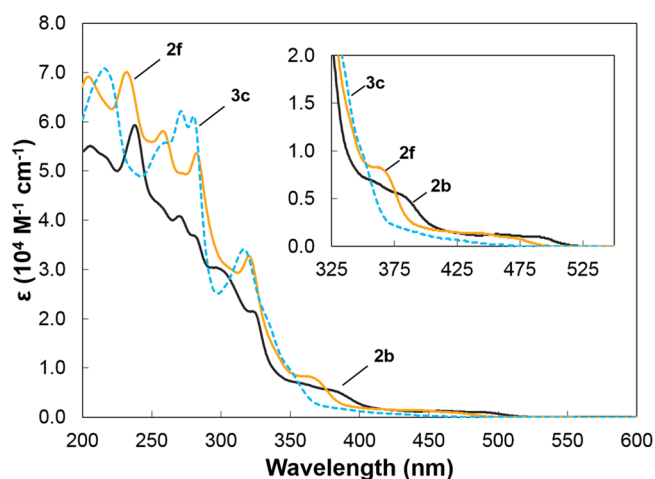


Figure 2. UV-vis absorption spectra for **2b** (solid black), **2f** (solid orange), and **3c** (dashed blue). All of the spectra were collected in acetonitrile (10 μ M) at room temperature.

nm (HOMO \rightarrow LUMO, mixed MLCT/ILCT) is present for all of the chloro complexes **2a–f** and is adjacent to stronger transition at 390 nm (HOMO-1 \rightarrow LUMO and HOMO \rightarrow LUMO+1, mixed MLCT/ILCT). Upon exchange of the chloride to a cyanide, these features disappear. TD-DFT calculations on **3c** indicate that these transitions, albeit weaker, are instead blue-shifted to 402 nm (HOMO \rightarrow LUMO, mixed MLCT/ILCT) and 343 nm (HOMO-2 \rightarrow LUMO and HOMO \rightarrow LUMO+2, mixed MLCT/ILCT), respectively. Subsequently, the region between 280 and 320 nm lacks any strong absorption bands for the chloro complexes with the exception of the perfluorinated complexes **2e** and **2f**. Two bands near 280 nm (HOMO-7 \rightarrow LUMO and HOMO-6 \rightarrow LUMO+1, mixed MLCT/ILCT) and 320 nm (HOMO-4 \rightarrow LUMO and HOMO-5 \rightarrow LUMO, mixed MLCT/ILCT) are prominent in these complexes, contrary to the spectra observed for previously published chloro analogues. Instead, this region bears similarities to that of the cyano complexes **3a–c**, which are characterized by mixed MLCT/ILCT transitions at 280 nm (HOMO-4 \rightarrow LUMO+1 and HOMO-3 \rightarrow LUMO+1) and 320 nm (HOMO-4 \rightarrow LUMO and HOMO-3 \rightarrow LUMO). The emergence of these features in **2e** and **2f** is likely due to the strong electron-withdrawing nature of the perfluorophenyl

moiety. Finally, a strong feature at 240 nm is present for all of the complexes, originating from an ILCT transition (ancillary ligand p orbitals, π orbitals of the central ring of the terpyridine, and π orbitals of the phenyl ring of the mppy to π^* orbitals of the terpyridine and π^* orbitals of the pyridine ring of the mppy). This feature is blue-shifted as the complexes increase in fluorination as well as upon exchange of a chloride to a cyanide because of increasing stabilization of the frontier orbitals.

Emission Spectroscopy. The complexes are strongly emissive in degassed room-temperature acetonitrile, with emission colors ranging from yellow to blue-green (Figure 3).

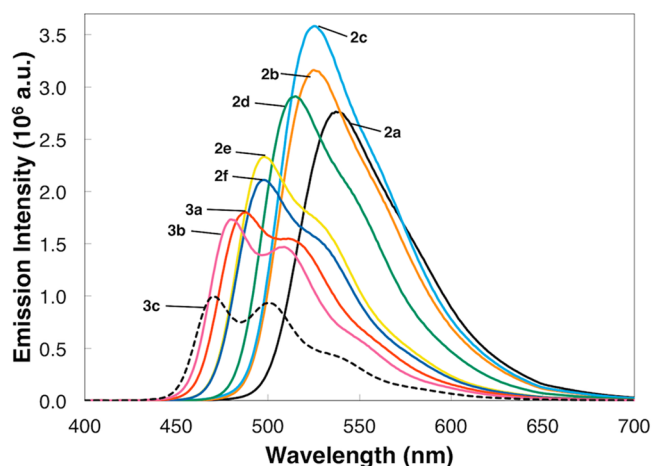


Figure 3. Room-temperature emission spectra of degassed 10 μ M solutions in acetonitrile. The complexes were excited at 380 nm. Vibrational substructure is visible in the spectra of complexes with predominantly ILCT transitions (**2e**, **2f**, and **3a–c**).

Complexes **2a–d** have broad, structureless emissions consistent with the mixed MLCT and ILCT character of cyclometallated iridium complexes. In contrast, complexes **2e**, **2f**, and **3a–c** have greater vibrational substructure in their emission, indicating a greater degree of ILCT emission than MLCT emission.

Increasing fluorination of the mppy ligand results in a blue shift of the emission maximum of the complex due to an increase in the stabilization of the HOMO. In a comparison of **2e** and **2f**, the emission maximum of the complex remains unchanged despite the addition of the methoxy group to **2f**.

Table 1. Photophysical Properties

complex	absorption $\lambda_{\text{max}}/\text{nm}$ (intensity/ $10^4 \text{ M}^{-1} \text{ cm}^{-1}$)	emission				
		$\lambda_{\text{max}}/\text{nm}$	$\tau^a/\mu\text{s}$	$\phi/\%$	$k_{\text{nr}}/10^5 \text{ s}^{-1}$	$k_{\text{r}}/10^5 \text{ s}^{-1}$
2a	237 (5.37), 256sh (3.75), 270 (3.55), 280sh (3.34), 303 (2.74), 326sh (1.71), 361 (0.61), 382sh (0.54), 465 (0.14)	537	3.02	60.7 \pm 5.2	1.30	2.01
2b	205 (5.50), 238 (5.93), 256sh (4.31), 269 (4.08), 277sh (3.74), 296sh (3.04), 323 (2.15), 381 (0.54), 450 (0.13)	525	3.17	64.6 \pm 5.5	1.12	2.04
2c	204 (5.41), 236 (6.32), 256sh (4.26), 269 (3.87), 282 (3.65), 302 (3.00), 323sh (2.10), 358 (0.62), 382 (0.57), 455 (0.13)	525	3.77	69.3 \pm 5.9	0.81	1.84
2d	206 (5.28), 237 (6.01), 257 (4.22), 268sh (3.81), 280 (3.40), 304sh (2.59), 323 (2.17), 375sh (0.57), 450 (0.14)	515	3.87	58.6 \pm 5.0	1.07	1.51
2e	203 (6.46), 232 (6.35), 252sh (5.05), 282 (4.34), 320sh (2.61), 366 (0.74), 436 (0.14)	498	3.05	50.0 \pm 4.3	1.64	1.64
2f	204 (6.91), 232 (7.01), 258 (5.81), 280 (5.27), 320 (3.27), 365 (0.81), 435 (0.14)	498	3.15	47.5 \pm 4.1	1.67	1.51
3a	216 (6.72), 238 (5.28), 271 (5.41), 280 (5.26), 316 (2.89), 430 (0.01)	488	3.35	55.8 \pm 5.1	1.32	1.67
3b	216 (6.69), 270 (5.28), 280 (4.89), 317 (3.02), 428 (0.01)	480	3.50	61.8 \pm 5.9	1.09	1.77
3c	216 (7.08), 255sh (5.49), 271 (6.21), 280 (6.11), 316 (3.40), 337sh (1.72),	470	9.93	41.4 \pm 4.2	0.59	0.42

^aExcited-state lifetimes were measured to within ± 50 ns.

Exchange of the chloride ligand to a cyanide also causes a blue shift in the emission maximum compared with the corresponding chloro analogue. As the mppy ligand is fluorinated, the HOMO–LUMO gap is broadened. A similar trend is seen in the cyano analogues 3a–c. It is worth noting that even though 2b and 2c are monofluorinated, they have higher quantum yields than the unsubstituted 2a. Compared with those of other common iridium complexes,³⁸ the excited-state lifetimes of the complexes are notably high, averaging 3.3 μ s, with the exception of 3c, whose lifetime is 3 times as long. The k_{nr} rate constants of 2a–3c are smaller than those of other published Ir(III) complexes with the [Ir(tpy)(ppy)X]⁺ ligand structure,⁷⁴ indicating that the complexes have more desirable photophysical properties (Figure 4). In addition, excluding 2e

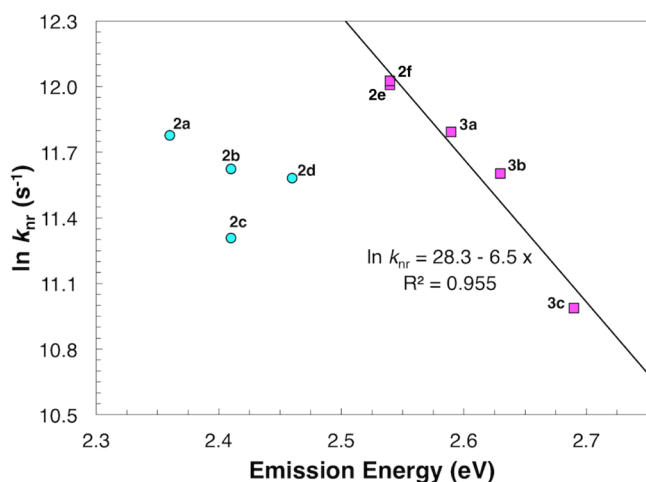


Figure 4. Energy gap law correlation of complexes 2a–3c. Cyan circles indicate complexes with emissions with mixed MLCT/ILCT character. Magenta squares indicate complexes with emissions having greater ILCT character. Differences in excited-state character are evident from the vibrational substructure of the luminescence spectra (Figure 3) as well as the grouping of these data points.

and 2f, all of the complexes have smaller k_{nr} than the most popular “push–pull” derivative of the [Ir(ppy)₂(bpy)]⁺ family, [Ir(dF(CF₃)ppy)₂(dtbbpy)]PF₆ ($k_{nr} = 1.39 \times 10^5 s^{-1}$).⁸⁹ The complexes also have large k_r rate constants, although they are smaller than that of [Ir(dF(CF₃)ppy)₂(dtbbpy)]PF₆ ($k_r = 2.96 \times 10^5 s^{-1}$). The overall high quantum efficiency of these complexes can be attributed to their “push–pull” design.

Analyzing the electronic structure of the singly occupied molecular orbitals (SOMOs) explains the changes in the emission structure and photophysical properties as the complexes increase in fluorination as well as upon exchange of the chloro ligand to a cyano ligand. As shown in Figure 1, 2c has a strong contribution of the iridium center in the electronic structures of its SOMOs. This high metal character and greater degree of spin–orbit coupling results in an emission that is primarily MLCT in nature, which is also seen in complexes 2b–d. In contrast, 3c has significantly less metal character in the SOMOs, resulting in an emission of 3c that is predominantly ILCT in nature. The presence of the corresponding transitions in the UV–vis spectra of the perfluorinated chloro complexes 2e and 2f, which are identical to those of the cyano complexes, also indicates a similarity in their excited states. The significantly longer excited-state lifetimes and lower quantum yields in comparison with other

complexes in the series is symptomatic of this switch in the nature of the excited state. It should also be noted that when the perfluorinated complexes 2e and 2f are analyzed in accordance to the energy gap law, their excited states behave similarly to those of the cyano complexes 3a–c, an observation that is highlighted in Figure 4.

DFT calculations have previously been utilized to predict the emission energies of Ir(III) complexes.^{38,90,91} One method involves calculating the energy difference of the singlet and triplet excited states at the optimized triplet geometry.^{38,91} This method has been successful with structurally diverse sets of iridium(III) complexes, but the dramatic differences in the characters of the excited states of 2a–3c tremendously diminished the accuracy of these predictions ($R^2 = 0.60$; see the Supporting Information). Instead, using the energy difference between the singlet ground states and triplet excited states at their respective optimized geometries results in a significant improvement in modeling the emission energies, especially given the diversity of excited states within this family of complexes ($R^2 = 0.96$; Figure 5).^{90,91}

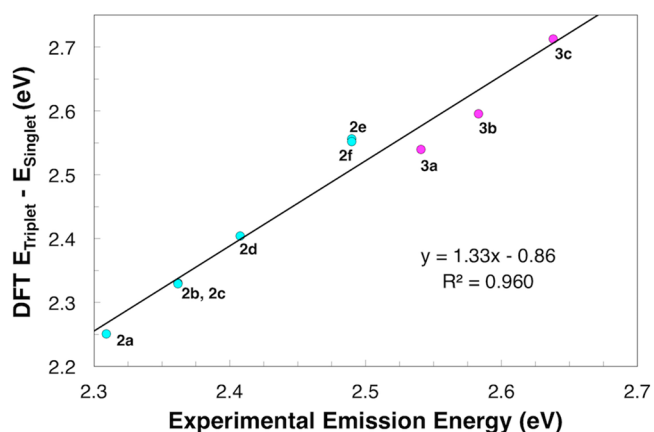


Figure 5. Relationship between experimental emission energy and the total energy difference between the singlet ground state and triplet excited state at their respective optimized geometries. Cyan circles indicate the chloro complexes 2a–f and magenta circles the cyano complexes 3a–c.

Electrochemical Characterization. Cyclic voltammetry experiments on the synthesized iridium compounds were performed in acetonitrile (Table 2). All of the complexes show only one oxidation that can be attributed to a metal-centered process with some involvement of the mppy ligand and the ancillary ligand. In the chloro complexes, the oxidation is quasi-reversible (Figure 6a), whereas in the cyano complexes the oxidation is irreversible (Figure 6b). Previous complexes from the [Ir(tpy)(ppy)X]⁺ family have shown up to two oxidations,^{74–77} but none had such a strong “push–pull” design as the complexes in this work, which results in increased electron density in the mppy and ancillary ligands. As fluorination increases in both the chloro and cyano complexes, the oxidation potential shifts in the positive direction as a result of stabilization of the HOMO on the mppy and ancillary ligands. In the cases of 2f and 3c, the addition of a methoxy group to the pyridine ring of the cyclometallating ligand results in a decrease in the oxidation potential, given its strongly electron-donating nature and participation in the HOMO. The oxidation potential is also shifted in the positive direction when

Table 2. Electrochemical Properties of Chloro Complexes 2a–f and Cyano Complexes 3a–c

compound	oxidation ^a		reduction ^a	
	E_{pa}/V	I: $E_{1/2}/V$ ($\Delta E/mV$)	II: E_{pc}/V	III: E_{red}/V
2a	1.61	-1.23 (45)	-1.69	-2.11
2b	1.70	-1.17 (65)	-1.63	-2.13
2c	1.69	-1.21 (69)	-1.68	-2.17
2d	1.87	-1.18 (38)	-1.62	-1.80
2e	1.88	-1.19 (51)	-1.65	-1.93
2f	1.83	-1.14 (97)	-1.63	-1.91

compound	oxidation ^a		reduction ^a	
	E_{pa}/V	I: $E_{1/2}/V$ ($\Delta E/mV$)	II: $E_{1/2}/V$ ($\Delta E/mV$)	
3a	1.95	-1.17 (68)	-1.74 (83)	
3b	1.73 (sh), 2.01	-1.17 (66)	-1.74 (86)	
3c	2.00	-1.17 (55)	-1.75 (81)	

^aPotentials were measured in acetonitrile using 0.10 M tetra-*n*-butylammonium hexafluorophosphate as the supporting electrolyte with 0.5 mM analyte. Cyclic voltammetry experiments were performed using a three-electrode system with positive scan polarity at 0.10 V/s under an atmosphere of argon using argon-purged solutions. Potentials are given in V vs SCE, and peak separations are given in mV.

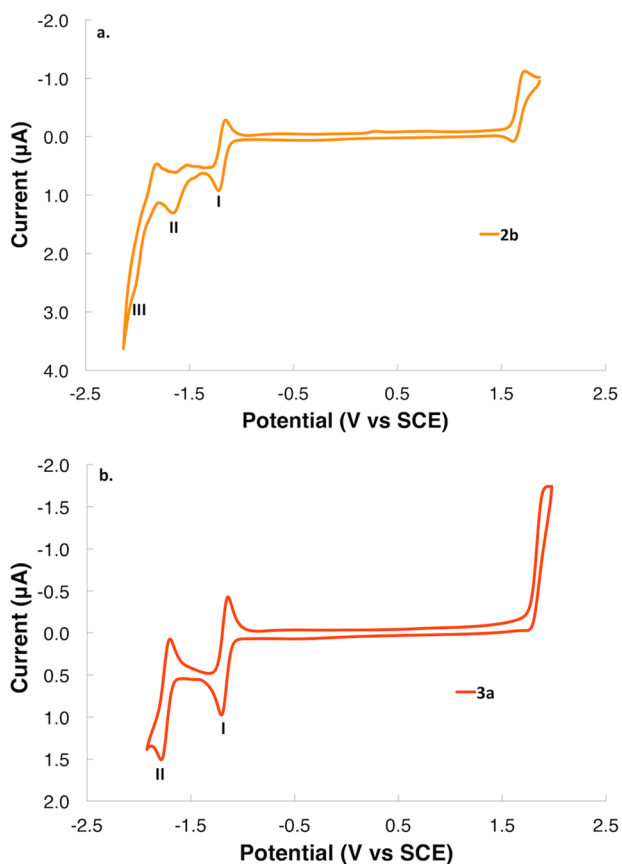


Figure 6. Cyclic voltammograms of (a) 2b and (b) 3a. Roman numerals indicate the unique reductions seen in the complexes. Voltammograms were recorded using argon-degassed 0.10 M tetra-*n*-butylammonium hexafluorophosphate (acetonitrile) solutions containing 0.5 mM analyte at 0.10 V/s with a three-electrode system. All of the potentials are referenced to SCE using ferrocene as an internal standard ($Fc/Fc^+ = 0.40$ V).⁸⁰

the chloride ligand is exchanged for a cyanide because of its stronger ligand-field character.

The first reduction observed for all of the complexes with the $[Ir(tpy)(ppy)X]^+$ configuration occurs on the terpyridine ligand. This reduction is completely reversible in all of the complexes studied. While the complexes all have the same 4,4',4''-tri-*tert*-butyl-2,2':6',2''-terpyridine ligand, differences in the first reduction potentials are still observed, arising from changes to the mppy and ancillary ligands. The absence of fluorine atoms in 2a results in a slightly lower reduction potential compared with those of the fluorinated analogues. In addition, it appears that the position of the fluorine atoms leads to differences in the reduction potential. Complex 2c, despite having the same number of fluorine atoms as 2b, has a noticeably lower reduction potential. This difference is likely due to the different meta position of the fluorine atom with respect to the cyclometallating carbon in 2c compared with 2b. Meanwhile the methoxy group in 2f increases the first reduction potential compared with that of the methyl analogue 2e, despite the fact that both are the most fluorinated. In contrast, the first reduction potential remains unchanged within the structurally different cyano complexes 3a–c.

The second reduction was assigned to the cyclometallating ligand of the Ir complexes. In the chloro complexes 2a–f, this reduction was found to be irreversible, whereas it is fully reversible in the cyano complexes 3a–c. Much like the first reduction, the second reduction of 2a occurs at a lower potential than those of the other complexes within the chloro series. Subsequently 2c's second reduction, much like its isomer 2b despite the same degree of fluorination of the phenyl ring. In addition, the methoxy group of 2f is responsible for the higher second reduction potential compared to the methyl analogue 2e. In contrast, the second reduction potential observed in the cyano complexes remains fairly unchanged by fluorination. Since the cyanide ligand has stronger back-bonding to the Ir(III) center than the chloride ligand, dissociation is unlikely, resulting in not only the reversibility of this reduction in the cyano complexes but also its stability regardless of ligand fluorination.

A third reduction is observed only in the chloro complexes 2a–f, and it is related to the dissociation of the chloride ligand. This reduction is irreversible, much like the second reduction in the chloro complexes. The loss of the chloride becomes more difficult as the complexes are substituted by one fluorine, and a small change is again observable in the different monofluorinated complexes 2b and 2c. However, the complexes with two or more fluorine atoms show the loss of the chloride to be significantly easier. Perfluorination seems to increase the third redox potential regardless of the substitution of the pyridine ring. Overall, difluorinated analogue 2d is the most susceptible to chloride loss.

From the redox potentials obtained by cyclic voltammetry and the emission maxima, excited-state redox potentials were determined in order to better evaluate the photosensitization properties of the complexes (Table 3).⁹² While the complexes' excited states are not as strongly reducing as that of $[Ir(dF(CF_3)ppy)_2(dtbbpy)]PF_6$, a known water-reducing catalyst⁸⁹ and "push-pull" photosensitizer, or the unsubstituted parent complex $[Ir(ppy)_2(bpy)]PF_6$,⁹³ the complexes are significantly stronger oxidants when excited.

Photocatalytic Hydrogen Evolution. Because of their appealing photochemical and electrochemical properties, the complexes were evaluated as photosensitizers for photocatalytic hydrogen evolution from water. The reactions were carried out

Table 3. Calculated Excited-State Redox Potentials⁹²

compound	$E([M^*]^+/[M]^{2+})/V^{a,b}$	$E([M^*]^+/[M]^0)/V^{a,c}$
2a	-0.70	1.07
2b	-0.66	1.19
2c	-0.67	1.15
2d	-0.54	1.22
2e	-0.61	1.30
2f	-0.66	1.35
3a	-0.59	1.37
3b	-0.57	1.42
3c	-0.64	1.47
[Ir(ppy) ₂ (bpy)]PF ₆ ⁹³	-0.85	0.68
[Ir(dF(CF ₃)ppy) ₂ (dtbbpy)]PF ₆ ⁸⁹	-0.89	1.21

^aPotentials are given in V vs SCE. ^b $E([M^*]^+/[M]^{2+}) = E_{ox} - E_{\lambda_{em}}$. ^c $E([M^*]^+/[M]^0) = E_{red} + E_{\lambda_{em}}$.

in 8:1 acetonitrile/water using K₂PtCl₄ as the water-reducing catalyst and triethylamine (TEA) as a sacrificial donor following previously established protocols.⁸⁵ The photocatalytic activity was determined against [Ir(dMeOphtpy)(4-Fmpy)Cl]PF₆, as it was the most structurally comparable and efficient photosensitizer in the literature⁷⁴ to date.

As indicated by the hydrogen evolution traces in Figure 7, a wide range of photosensitizing abilities was observed with the

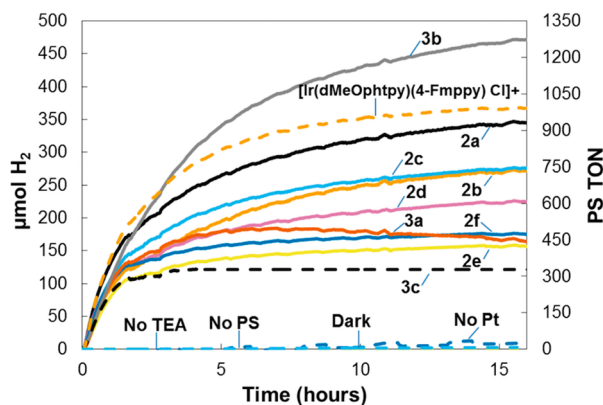


Figure 7. Performance of complexes 2a–3c as photosensitizers for photocatalytic hydrogen evolution. The amounts of hydrogen evolved (in μmol) are noted along with the turnover numbers (TONs) of the Ir(III) photosensitizers. Control experiments are indicated.

new complexes. Complex 3b was found to be the best performer, clearly outclassing [Ir(dMeOphtpy)(4-Fmpy)Cl]PF₆.⁷⁴ 3b's stronger "push-pull" structure and the enhanced luminescence quantum yield compared with [Ir(dMeOphtpy)(4-Fmpy)Cl]PF₆ are contributing factors to this increase in performance. The performance of the chlorinated compounds (2a–f) indicates that decreasing fluorination leads to higher photosensitizing ability. This can be rationalized on the basis of the fact that the complexes with less-electron-withdrawing cyclometalating ligands had increased metal character in their excited states. The cyano complexes 3a–c followed a similar trend in which the metal character in the excited state (see the Supporting Information) as well as a higher k_{nr}/k_r ratio and consequently a higher luminescence quantum yield were correlated with increased hydrogen production. Comparisons between the chloro and cyano series are difficult because of the change in the nature of the excited state from mixed MLCT/ILCT in the chloro series to purely ILCT in the cyano series. However, it can be noted that compounds 2e, 2f, and 3a all had

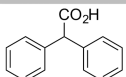
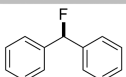
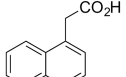
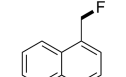
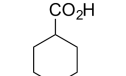
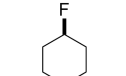
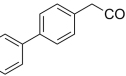
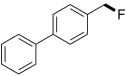
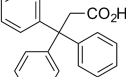
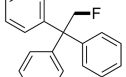
very similar excited-state properties and performed comparably in photocatalytic hydrogen evolution studies.

Photoredox Catalysis. Complexes 2b and 3a were evaluated as photosensitizers for the photocatalytic decarboxylative fluorination of carboxylic acids. Previous studies have shown that [Ir(ppy)₂(bpy)]⁺-based photosensitizers can catalyze several organic transformations.^{40–48} Much like photocatalytic water reduction, photocatalytic decarboxylative fluorination relies on the photogeneration of a highly reducing Ir(III)* species, which upon oxidative quenching with an electron acceptor produces a transient Ir(IV) species. This can go on to react with a deprotonated carboxylic acid to generate CO₂, the now-regenerated Ir(III) photocatalyst, and a radical species that proceeds to react with the fluorine source, Selectfluor.⁸⁶ Since 2a and 3b were proven to generate hydrogen from water photocatalytically, their use as photosensitizers for the photocatalytic decarboxylative fluorination was a novel path to follow.

The performance of 2b, 3a, and the cited best photosensitizer for this transformation, [Ir(dF(CF₃)ppy)₂(dtbbpy)]PF₆,⁸⁶ was evaluated using the decarboxylative fluorination of five carboxylic acids, as shown in Table 4. MacMillan's original protocol called for a 1 mol % catalyst loading.⁸⁶ However, to better evaluate whether 2b and 3a were more stable in the highly coordinating solvent of the reaction (3:1 acetonitrile/water), a concentration study with 2b was performed (see the Supporting Information). It was determined that up to a 100-fold reduction of catalyst still gave comparable performance based on CO₂ evolution, and therefore, a 20-fold-reduced catalyst loading of 0.05 mol % for all three catalysts was used for subsequent reactions. Reaction yields were determined by ¹⁹F NMR spectroscopy using hexafluorobenzene as an internal standard. The NMR signals of the products matched those reported in the literature (fluorodiphenylmethane,⁹⁴ 1-(fluoromethyl)naphthalene,⁹⁵ fluorocyclohexane,⁹⁶ 4-(fluoromethyl)-1,1'-biphenyl, and 2-fluoro-1,1,1-triphenylethane⁸⁶). Control reactions in which the catalyst, base, or light was omitted did not generate the fluorinated products.

The yields of the reactions with 2b and 3a were comparable to each other in most cases, while the yields with [Ir(dF(CF₃)ppy)₂(dtbbpy)]PF₆ under the same reaction conditions were noticeably lower. The CO₂ evolution of the reactions was also monitored over time, as shown in Figure 8 (additional traces are shown in the Supporting Information). In most cases, complexes 2b and 3a were shown to outperform [Ir(dF(CF₃)ppy)₂(dtbbpy)]PF₆. It would appear that the decrease in catalyst loading from 1 to 0.05 mol % had a more dramatic

Table 4. Photosensitizer and Substrate Studies of the Decarboxylative Fluorination Reaction

R-CO ₂ H	R-F	yield (%) ^a		
		2b	3a	[Ir(dF(CF ₃)ppy) ₂ (dtbbpy)]PF ₆
		58	57	44
		37	41	40
		10	13	3
		99	63	4
		61	57	23

^aDetermined by ¹⁹F NMR analysis using hexafluorobenzene as an internal standard.

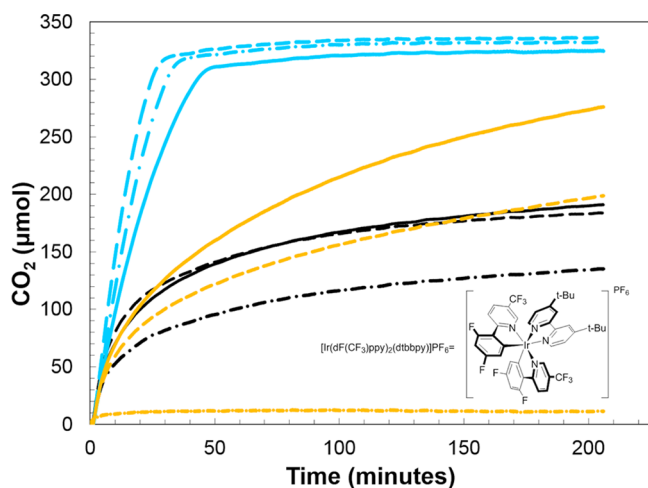


Figure 8. Performance of complexes **2b** (solid lines), **3a** (dashed lines), and [Ir(dF(CF₃)ppy)₂(dtbbpy)]PF₆ (dot-dashed lines) as photosensitizers for decarboxylative fluorination of 1-naphthaleneacetic acid (blue), 4-biphenylacetic acid (gold), and diphenylacetic acid (black). The amounts of CO₂ evolved are noted.

effect on the performance of [Ir(dF(CF₃)ppy)₂(dtbbpy)]PF₆. This can be explained by the differences in the ligand structures, specifically that the terpyridine–phenylpyridine structure imparts significantly greater stability than the traditional [Ir(ppy)₂(bpy)]⁺ design, which is known to degrade in highly coordinating solvents (including acetonitrile) over periods of time.^{39,97} Also, the excited-state lifetimes of **2b** and **3a** (3.17 and 3.35 μs, respectively) are both longer than that of [Ir(dF(CF₃)ppy)₂(dtbbpy)]PF₆ (2.3 μs),⁸⁹ which allows greater time for the photoinduced transfer of electrons necessary for the transformation. While it has been shown through electrochemical experiments that the cyano complexes are more stable than the chloro analogues, this does not account for instance where the performance of **2b** was significantly greater than that of **3a**, specifically, 4-biphenylacetic acid.

Instead, the difference in the excited-state oxidation potentials of the complexes could explain the difference in reactivity, with **2b** being less oxidizing than **3a**. Future analysis of the electrochemistry of the carboxylates could provide additional insight.

CONCLUSION

A series of Ir(III) luminophores using the recently published [Ir(tpy)(ppy)X]⁺ ligand framework were synthesized via C–F activation, a highly unusual process. The synthesis was accomplished using symmetrical fluorinated phenylpyridine ligands that preferentially activated C–F bonds, with trace formation of the C–H activation products. The addition of strongly electron-donating *tert*-butyl groups to the terpyridine ligand tuned the LUMO of the complex, whereas variation in the degree of fluorination of the cyclometallating ligand and exchange of the ancillary ligand successfully tuned the HOMO. This combination resulted in efficient photochemical performance marked by high quantum yields and long excited-state lifetimes. As the complexes had greater degrees of fluorination, a change in the nature of the excited state was observed, gradually increasing in ILCT character and decreasing in MLCT character. This resulted in performance in photocatalytic hydrogen evolution that was mixed compared with previous compounds but nonetheless still impressive given the highly coordinating conditions of that reaction. When used as a photosensitizer for decarboxylative fluorination of several carboxylic acids, two of the complexes outperformed the state-of-the-art photosensitizer for the reaction. In view of the improvements imparted by the “push–pull” design of the complexes, future work on implementing these compounds into applications where characteristics such as high quantum efficiencies and photochemical stability are highly desirable should be explored.

ASSOCIATED CONTENT

Supporting Information

The Supporting Information is available free of charge on the ACS Publications website at DOI: 10.1021/jacs.6b03246.

Synthetic procedures and characterization of the cyclometallating ligands (NMR and ESI-MS), the corresponding precursors, and the final complexes; DFT results for the complexes (optimized singlet geometry coordinates, HOMO and LUMO energy levels, TD-DFT results, and triplet frontier orbitals for **3a–c**) and results from modeling of the excited states and emission maxima; ESI-MS and ¹⁹F NMR data for crude reactions; ¹H NMR data for 2,4-dinitrophenylhydrazine derivatizations; and additional CO₂ evolution traces (PDF)

AUTHOR INFORMATION

Corresponding Author

*bern@cmu.edu

Notes

The authors declare no competing financial interest.

ACKNOWLEDGMENTS

The authors acknowledge support from the National Science Foundation through CHE-1362629. NMR instrumentation at CMU was partially supported by the NSF (CHE-0130903 and CHE-1039870).

REFERENCES

- (1) Ahrens, T.; Kohlmann, J.; Ahrens, M.; Braun, T. *Chem. Rev.* **2015**, *115*, 931–972.
- (2) Weaver, J.; Senaweera, S. *Tetrahedron* **2014**, *70*, 7413–7428.
- (3) Richmond, T. G.; Osterberg, C. E.; Arif, A. M. *J. Am. Chem. Soc.* **1987**, *109*, 8091–8092.
- (4) Kiplinger, J. L.; Richmond, T. G.; Osterberg, C. E. *Chem. Rev.* **1994**, *94*, 373–431.
- (5) Braun, T.; Perutz, R. N. *Chem. Commun.* **2002**, 2749–2757.
- (6) Hughes, R. P.; Smith, J. M.; Incarvito, C. D.; Lam, K. C.; Rhatigan, B.; Rheingold, A. L. *Organometallics* **2002**, *21*, 2136–2144.
- (7) Hughes, R. P.; Laritchev, R. B.; Williamson, A.; Incarvito, C. D.; Zakharov, L. N.; Rheingold, A. L. *Organometallics* **2002**, *21*, 4873–4885.
- (8) Jones, W. D. *Dalton Trans.* **2003**, 3991–3995.
- (9) Mazurek, U.; Schwarz, H. *Chem. Commun.* **2003**, 1321–1326.
- (10) Torrens, H. *Coord. Chem. Rev.* **2005**, *249*, 1957–1985.
- (11) Amii, H.; Uneyama, K. *Chem. Rev.* **2009**, *109*, 2119–2183.
- (12) Menjón, B.; Martínez-Salvador, S.; Gómez-Saso, M. A.; Forniés, J.; Falvello, L. R.; Martín, A.; Tsipis, A. *Chem. - Eur. J.* **2009**, *15*, 6371–6382.
- (13) Crespo, M. *Organometallics* **2012**, *31*, 1216–1234.
- (14) Reinhold, M.; McGrady, J. E.; Perutz, R. N. *J. Am. Chem. Soc.* **2004**, *126*, 5268–5276.
- (15) Selmeczy, A. D.; Jones, W. D.; Partridge, M. G.; Perutz, R. N. *Organometallics* **1994**, *13*, 522–532.
- (16) Bosque, R.; Clot, E.; Fantacci, S.; Maseras, F.; Eisenstein, O.; Perutz, R. N.; Renkema, K. B.; Caulton, K. G. *J. Am. Chem. Soc.* **1998**, *120*, 12634–12640.
- (17) Barrio, P.; Castarlenas, R.; Esteruelas, M. A.; Lledos, A.; Maseras, F.; Onate, E.; Tomas, J. *Organometallics* **2001**, *20*, 442–452.
- (18) Albéniz, A. C.; Calle, V.; Espinet, P.; Gómez, S. *Chem. Commun.* **2002**, 610–611.
- (19) Fan, L.; Parkin, S.; Ozerov, O. V. *J. Am. Chem. Soc.* **2005**, *127*, 16772–16773.
- (20) Salomon, M. A.; Braun, T.; Krossing, I. *Dalton Trans.* **2008**, *5*, 5197–5206.
- (21) Kläring, P.; Jungton, A. K.; Braun, T.; Müller, C. *Eur. J. Inorg. Chem.* **2012**, *2012*, 1430–1436.
- (22) Baumgarth, H.; Braun, T.; Braun, B.; Laubenstein, R.; Herrmann, R. *Eur. J. Inorg. Chem.* **2015**, *2015*, 3157–3168.
- (23) Blum, O.; Frolow, F.; Milstein, D. *J. Chem. Soc., Chem. Commun.* **1991**, *0*, 258–259.
- (24) Fawcett, J.; Friedrichs, S.; Holloway, J. H.; Hope, E. G.; McKee, V.; Nieuwenhuyzen, M.; Russell, D. R.; Saunders, G. C. *J. Chem. Soc., Dalton Trans.* **1998**, 1477–1484.
- (25) Godoy, F.; Higgitt, C. L.; Klahn, A. H.; Oelckers, B.; Parsons, S.; Perutz, R. N. *J. Chem. Soc., Dalton Trans.* **1999**, 2039–2048.
- (26) Erhardt, S.; Macgregor, S. A. *J. Am. Chem. Soc.* **2008**, *130*, 15490–15498.
- (27) Li, L.; Wu, F.; Zhang, S.; Wang, D.; Ding, Y.; Zhu, Z. *Dalton Trans.* **2013**, *42*, 4539–4543.
- (28) Nakai, H.; Jeong, K.; Matsumoto, T.; Ogo, S. *Organometallics* **2014**, *33*, 4349–4352.
- (29) Procacci, B.; Jiao, Y.; Evans, M. E.; Jones, W. D.; Perutz, R. N.; Whitwood, A. C. *J. Am. Chem. Soc.* **2015**, *137*, 1258–1272.
- (30) You, Y.; Cho, S.; Nam, W. *Inorg. Chem.* **2014**, *53*, 1804–1815.
- (31) Huang, H.; Yang, L.; Zhang, P.; Qiu, K.; Huang, J.; Chen, Y.; Diao, J.; Liu, J.; Ji, L.; Long, J.; Chao, H. *Biomaterials* **2016**, *83*, 321–331.
- (32) Lo, K. K. W.; Chung, C. K.; Lee, T. K. M.; Lui, L. H.; Tsang, K. H. K.; Zhu, N. *Inorg. Chem.* **2003**, *42*, 6886–6897.
- (33) Lo, K. K. W.; Hui, W. K.; Chung, C. K.; Tsang, K. H. K.; Lee, T. K. M.; Li, C. K.; Lau, J. S. Y.; Ng, D. C. M. *Coord. Chem. Rev.* **2006**, *250*, 1724–1736.
- (34) Lo, K. K.-W.; Tsang, K. H.-K.; Sze, K.-S.; Chung, C.-K.; Lee, T. K. M.; Zhang, K. Y.; Hui, W.-K.; Li, C.-K.; Lau, J. S.-Y.; Ng, D. C.-M.; Zhu, N. *Coord. Chem. Rev.* **2007**, *251*, 2292–2310.
- (35) Yu, M.; Zhao, Q.; Shi, L.; Li, F.; Zhou, Z.; Yang, H.; Yi, T.; Huang, C. *Chem. Commun.* **2008**, 2115–2117.
- (36) Millett, A. J.; Habtemariam, A.; Romero-Canelón, I.; Clarkson, G. J.; Sadler, P. J. *Organometallics* **2015**, *34*, 2683–2694.
- (37) Lowry, M. S.; Bernhard, S. *Chem. - Eur. J.* **2006**, *12*, 7970–7977.
- (38) Lowry, M. S.; Hudson, W. R.; Pascal, R. A.; Bernhard, S. *J. Am. Chem. Soc.* **2004**, *126*, 14129–14135.
- (39) Tinker, L. L.; McDaniel, N. D.; Curtin, P. N.; Smith, C. K.; Ireland, M. J.; Bernhard, S. *Chem. - Eur. J.* **2007**, *13*, 8726–8732.
- (40) Prier, C. K.; Rankic, D. A.; MacMillan, D. W. C. *Chem. Rev.* **2013**, *113*, 5322–5363.
- (41) Skubi, K. L.; Blum, T. R.; Yoon, T. P. *Chem. Rev.* **2016**, DOI: 10.1021/acs.chemrev.6b00018.
- (42) Zuo, Z.; Cong, H.; Li, W.; Choi, J.; Fu, G. C.; MacMillan, D. W. C. *J. Am. Chem. Soc.* **2016**, *138*, 1832–1835.
- (43) Le, C.; MacMillan, D. W. C. *J. Am. Chem. Soc.* **2015**, *137*, 11938–11941.
- (44) Nawrat, C. C.; Jamison, C. R.; Slutskyy, Y.; MacMillan, D. W. C.; Overman, L. E. *J. Am. Chem. Soc.* **2015**, *137*, 11270–11273.
- (45) Scholz, S. O.; Farney, E. P.; Kim, S.; Bates, D. M.; Yoon, T. P. *Angew. Chem., Int. Ed.* **2016**, *55*, 2239–2242.
- (46) Amador, A. G.; Yoon, T. P. *Angew. Chem., Int. Ed.* **2016**, *55*, 2304–2306.
- (47) Hurlley, A. E.; Lu, Z.; Yoon, T. P. *Angew. Chem., Int. Ed.* **2014**, *53*, 8991–8994.
- (48) Lu, Z.; Yoon, T. P. *Angew. Chem., Int. Ed.* **2012**, *51*, 10329–10332.
- (49) Bezzubov, S. I.; Kiselev, Y. M.; Churakov, A. V.; Kozyukhin, S. A.; Sadovnikov, A. A.; Grinberg, V. A.; Emets, V. V.; Doljenko, V. D. *Eur. J. Inorg. Chem.* **2016**, *2016*, 347–354.
- (50) Zanon, K. P. S.; Coppo, R. L.; Amaral, R. C.; Iha, N. Y. M. *Dalton Trans.* **2015**, *44*, 14559–14573.
- (51) Baranoff, E.; Yum, J. H.; Graetzl, M.; Nazeeruddin, M. K. J. *Organomet. Chem.* **2009**, *694*, 2661–2670.
- (52) González, I.; Cortés-Arriagada, D.; Dreyse, P.; Sanhueza-Vega, L.; Ledoux-Rak, I.; Andrade, D.; Brito, I.; Toro-Labbé, A.; Soto-Arriaza, M.; Caramori, S.; Loeb, B. *Eur. J. Inorg. Chem.* **2015**, *2015*, 4946–4955.
- (53) Lamansky, S.; Djurovich, P.; Murphy, D.; Abdel-Razzaq, F.; Lee, H. E.; Adachi, C.; Burrows, P. E.; Forrest, S. R.; Thompson, M. E. *J. Am. Chem. Soc.* **2001**, *123*, 4304–4312.
- (54) You, Y.; Park, S. Y. *Dalton Trans.* **2009**, 9226, 1267–1282.
- (55) Tordera, D.; Bunzli, A. M.; Pertegas, A.; Junquera-Hernandez, J. M.; Constable, E. C.; Zampese, J. A.; Housecroft, C. E.; Orti, E.; Bolink, H. J. *Chem. - Eur. J.* **2013**, *19*, 8597–8609.
- (56) Constable, E. C.; Ertl, C. D.; Housecroft, C. E.; Zampese, J. A. *Dalton Trans.* **2014**, *43*, 5343–5356.
- (57) Coppo, P.; Plummer, A.; De Cola, L. *Chem. Commun.* **2004**, 1774–1775.
- (58) Grushin, V. V.; Herron, N.; LeCloux, D. D.; Marshall, W. J.; Petrov, V. a; Wang, Y. *Chem. Commun.* **2001**, 1494–1495.
- (59) Takizawa, S. Y.; Nishida, J. I.; Tsuzuki, T.; Tokito, S.; Yamashita, Y. *Inorg. Chem.* **2007**, *46*, 4308–4310.
- (60) Xu, M.; Zhou, R.; Wang, G.; Xiao, Q.; Du, W.; Che, G. *Inorg. Chim. Acta* **2008**, *361*, 2407–2412.
- (61) Liu, C.; Lv, X.; Xing, Y.; Qiu, J. *J. Mater. Chem. C* **2015**, *3*, 8010–8017.
- (62) Li, H.; Zhou, L.; Teng, M.; Xu, Q.; Lin, C.; Zheng, Y.; Zuo, J.; Zhang, H.; You, X. *J. Mater. Chem. C* **2013**, *1*, 560–565.
- (63) Li, H.-Y.; Li, T.; Teng, M.; Xu, Q.; Zhang, S.; Jin, Y.; Liu, X.; Zheng, Y.-X.; Zuo, J.-L. *J. Mater. Chem. C* **2014**, *2*, 1116–1124.
- (64) Li, T. Y.; Liang, X.; Wu, C.; Xue, L. S.; Xu, Q. L.; Zhang, S.; Liu, X.; Zheng, Y. X.; Wang, X. Q. *J. Organomet. Chem.* **2014**, *755*, 110–119.
- (65) Shavaleev, N. M.; Xie, G.; Varghese, S.; Cordes, D. B.; Slawin, A. M. Z.; Momblona, C.; Orti, E.; Bolink, H. J.; Samuel, I. D. W.; Zysman-Colman, E. *Inorg. Chem.* **2015**, *54*, 5907–5914.
- (66) Shavaleev, N. M.; Monti, F.; Scopelliti, R.; Armaroli, N.; Grätzel, M.; Nazeeruddin, M. K. *Organometallics* **2012**, *31*, 6288–6296.

- (67) Mills, I. N.; Kagalwala, H. N.; Chirdon, D. N.; Brooks, A. C.; Bernhard, S. *Polyhedron* **2014**, *33*, 104–108.
- (68) Niu, Z. G.; Liu, D.; Li, D. C.; Zuo, J.; Yang, J. M.; Su, Y. H.; Yang, Y. D.; Li, G. N. *Inorg. Chem. Commun.* **2014**, *17*, 146–150.
- (69) Lee, S.; Kim, S.-O.; Shin, H.; Yun, H.-J.; Yang, K.; Kwon, S.-K.; Kim, J.-J.; Kim, Y.-H. *J. Am. Chem. Soc.* **2013**, *135*, 14321–14328.
- (70) Ragni, R.; Plummer, E. A.; Brunner, K.; Hofstraat, J. W.; Babudri, F.; Farinola, G. M.; Naso, F.; De Cola, L. *J. Mater. Chem.* **2006**, *16*, 1161–1170.
- (71) Park, J.; Park, J. S.; Park, Y. G.; Lee, J. Y.; Kang, J. W.; Liu, J.; Dai, L.; Jin, S.-H. *Org. Electron.* **2013**, *14*, 2114–2123.
- (72) Ikeda, Y.; Kodama, S.; Tsuchida, N.; Ishii, Y. *Dalton Trans.* **2015**, *44*, 17448–17452.
- (73) Guo, W.-H.; Min, Q.-Q.; Gu, J.-W.; Zhang, X. *Angew. Chem., Int. Ed.* **2015**, *54*, 9075–9078.
- (74) Chirdon, D. N.; Transue, W. J.; Kagalwala, H. N.; Kaur, A.; Maurer, A. B.; Pintauer, T.; Bernhard, S. *Inorg. Chem.* **2014**, *53*, 1487–1499.
- (75) Reithmeier, R. O.; Meister, S.; Rieger, B.; Siebel, A.; Tschurl, M.; Heiz, U.; Herdtweck, E. *Dalton Trans.* **2014**, *43*, 13259–13269.
- (76) Reithmeier, R. O.; Meister, S.; Siebel, A.; Rieger, B. *Dalton Trans.* **2015**, *44*, 6466–6472.
- (77) Sato, S.; Morikawa, T.; Kajino, T.; Ishitani, O. *Angew. Chem., Int. Ed.* **2013**, *52*, 988–992.
- (78) Garg, K.; Matsubara, Y.; Ertem, M. Z.; Lewandowska-Andralojc, A.; Sato, S.; Szalda, D. J.; Muckerman, J. T.; Fujita, E. *Angew. Chem., Int. Ed.* **2015**, *54*, 14128–14132.
- (79) Do, H.-Q.; Daugulis, O. *J. Am. Chem. Soc.* **2008**, *130*, 1128–1129.
- (80) Connelly, N. G.; Geiger, W. E. *Chem. Rev.* **1996**, *96*, 877–910.
- (81) Frisch, M. J.; Trucks, G. W.; Schlegel, H. B.; Scuseria, G. E.; Robb, M. A.; Cheeseman, J. R.; Scalmani, G.; Barone, V.; Mennucci, B.; Petersson, G. A.; Nakatsuji, H.; Caricato, M.; Li, X.; Hratchian, H. P.; Izmaylov, A. F.; Bloino, J.; Zheng, G.; Sonnenberg, J. L.; Hada, M.; Ehara, M.; Toyota, K.; Fukuda, R.; Hasegawa, J.; Ishida, M.; Nakajima, T.; Honda, Y.; Kitao, O.; Nakai, H.; Vreven, T.; Montgomery, J. A., Jr.; Peralta, J. E.; Ogliaro, F.; Bearpark, M.; Heyd, J. J.; Brothers, E.; Kudin, K. N.; Staroverov, V. N.; Kobayashi, R.; Normand, J.; Raghavachari, K.; Rendell, A.; Burant, J. C.; Iyengar, S. S.; Tomasi, J.; Cossi, M.; Rega, N.; Millam, J. M.; Klene, M.; Knox, J. E.; Cross, J. B.; Bakken, V.; Adamo, C.; Jaramillo, J.; Gomperts, R.; Stratmann, R. E.; Yazyev, O.; Austin, A. J.; Cammi, R.; Pomelli, C.; Ochterski, J. W.; Martin, R. L.; Morokuma, K.; Zakrzewski, V. G.; Voth, G. A.; Salvador, P.; Dannenberg, J. J.; Dapprich, S.; Daniels, A. D.; Farkas, Ö.; Foresman, J. B.; Ortiz, J. V.; Cioslowski, J.; Fox, D. J. *Gaussian 09*, revision E.01; Gaussian, Inc.: Wallingford, CT, 2009.
- (82) Hanwell, M. D.; Curtis, D. E.; Lonie, D. C.; Vandermeersch, T.; Zurek, E.; Hutchison, G. R. *J. Cheminf.* **2012**, *4*, 17.
- (83) O'Boyle, N. M.; Tenderholt, A. L.; Langner, K. M. *J. Comput. Chem.* **2008**, *29*, 839–845.
- (84) Caspar, J. V.; Meyer, T. J. *J. Am. Chem. Soc.* **1983**, *105*, 5583–5590.
- (85) Cline, E. D.; Adamson, S. E.; Bernhard, S. *Inorg. Chem.* **2008**, *47*, 10378–10388.
- (86) Ventre, S.; Petronijevic, F. R.; MacMillan, D. W. C. *J. Am. Chem. Soc.* **2015**, *137*, 5654–5657.
- (87) Hartman, J. S.; Shoemaker, J. A. W.; Janzen, A. F.; Ragogna, P. J.; Szerminski, W. R. *J. Fluorine Chem.* **2003**, *119*, 125–139.
- (88) Hartmeyer, G.; Marichal, C.; Lebeau, B.; Cautlet, P.; Hernandez, J. J. *Phys. Chem. C* **2007**, *111*, 6634–6644.
- (89) Lowry, M. S.; Goldsmith, J. I.; Slinker, J. D.; Pascal, R. A.; Malliaras, G. G.; Bernhard, S.; Rohl, R. *Chem. Mater.* **2005**, *17*, 5712–5719.
- (90) Ladouceur, S.; Fortin, D.; Zysman-Colman, E. *Inorg. Chem.* **2011**, *50*, 11514–11526.
- (91) Donato, L.; Abel, P.; Zysman-Colman, E. *Dalton Trans.* **2013**, *42*, 8402–8412.
- (92) Kalyanasundaram, K. *Photochemistry of Polypyridine and Porphyrin Complexes*; Academic Press: New York, 1992.
- (93) Goldsmith, J. I.; Hudson, W. R.; Lowry, M. S.; Anderson, T. H.; Bernhard, S. *J. Am. Chem. Soc.* **2005**, *127*, 7502–7510.
- (94) Johnson, A. L. *J. Org. Chem.* **1982**, *47*, S220–S222.
- (95) Blessley, G.; Holden, P.; Walker, M.; Brown, J. M.; Gouverneur, V. *Org. Lett.* **2012**, *14*, 2754–2757.
- (96) Xia, J.-B.; Zhu, C.; Chen, C. *Chem. Commun.* **2014**, *50*, 11701–11704.
- (97) Curtin, P. N.; Tinker, L. L.; Burgess, C. M.; Cline, E. D.; Bernhard, S. *Inorg. Chem.* **2009**, *48*, 10498–10506.